

# Composition and Strain in InGaAs Quantum Dots

*A methodology based on grazing-incidence resonant x-ray diffraction has been developed for the high-resolution determination of spatial distribution of composition and strain in self-assembled InGaAs quantum dots grown on GaAs substrate. Near resonant conditions, the weak Bragg reflections are found to have distinct features, which can be applied to differentiate diffraction contributions from specific regions (iso-composition and iso-strain slabs, the regions with respectively constant compositions and lattice parameters) of dots. The methodology therefore provides a high-resolution sectioning scan for the dot structure. The structure reconstruction of dots has shown that the curvature of the iso-strain slabs exceeds that of the iso-composition slabs.*

Quantum dots (QDs), exhibiting confinements of electronic carriers, have been a major focus of research interest in the last decade. For semiconductor systems, the fabrication techniques of different QDs have been well developed to the extent that electronic and optoelectronic devices can be commercialized. Among which, the most effective way of fabricating semiconductor QDs is by self-assembled growth mechanism. Relying on the strain induced island formation via a Stranski-Krastanov growth mode, QDs so fabricated can be dislocation free and often exhibit a preferred shape and a narrow size distribution. Although fabrication techniques for various dots have greatly advanced, our knowledge of QDs, concerning the kinetic effect and equilibrium properties of formation and equilibrium, remains limited. Compared to the well-developed concepts of equilibrium crystal shape and surface segregation for bulk crystals, the understanding of the QD formation is still in an early stage. The limitation is partially due to the lack of quantitative structural probes, which are critically needed in advancing the QD research.

In this work, we report the results of x-ray studies of the InGaAs/GaAs QDs structure, using the grazing incidence resonant x-ray diffraction together with the distorted-wave Born approximation (DWBA) analysis. For the InGaAs/GaAs system of a zinc-blende structure, the weak reflections of Miller indices  $h + k + l = 4n + 2$  are highly sensitive to the composition change, in contrast to strong reflections, due to the small amplitude of the corresponding structure factor

$$F_{\text{InGaAs}}(\mathbf{Q}, E, x) = [xF_{\text{InAs}}(\mathbf{Q}, E) + (1-x)F_{\text{GaAs}}(\mathbf{Q}, E)] \\ = 4[xf_{\text{In}}(\mathbf{Q}, E) + (1-x)f_{\text{Ga}}(\mathbf{Q}, E) \pm f_{\text{As}}(\mathbf{Q}, E)], \quad (1)$$

where  $F$ 's and  $f$ 's are the structure factors and the atomic scattering factors with the plus and minus signs for strong and weak even (in Miller indices) reflections, respectively. We emphasize that the negative sign of  $f_{\text{As}}$  in (1) for weak reflections has

the decisive influence in reducing the magnitude of  $F_{\text{InGaAs}}$ . Moreover, in the approximation of an unabsorbed crystal,  $F_{\text{InGaAs}}$  as a function of  $x$  may change its values from the negative to the positive crossing the zero value (contrast-matching point with the minimum of amplitude). Then, the small  $F_{\text{InGaAs}}$  can be dominated by  $x$ , especially near the contrast matching point. The structural factor can be modulated by the reflection orders ( $\mathbf{Q}$ -dependence) or incident x-ray energy ( $E$ -dependence). The  $F(\mathbf{Q}, E, x)$  modulation can be further detailed by the atomic scattering factor  $f(\mathbf{Q}, E) = f_0(\mathbf{Q}) + f'(E) + f''(E)$ , consisting the non-resonant Thompson scattering factor  $f_0$ , the resonant scattering factors  $f'$  and  $f''$  that are responsible for the x-ray absorption. Near the absorption edges,  $f'$  and  $f''$  make a rather large contribution to the atomic scattering factors and vary drastically with the photon energy. Moreover, for weak reflections,  $f'$  and  $f''$  dominate in structure factors. For slabs with different composition, the resonant condition for minimum  $|F_{\text{InGaAs}}(x)|$  can be tuned through photon energy. In insert (a) of Fig. 1, we show the composition-dependent  $|F_{\text{InGaAs}}(x)|$  profiles calculated for the weak reflection (200) at energies in the vicinity of the Ga  $K$ -edge respectively, with the different  $x$  positions of minimum. In contrast,  $|F_{\text{InGaAs}}(x)|$  profiles in the insert (b) of Fig. 1, calculated for the strong reflection (400), are not as sensitive to the same energy change as that observed in the insert (a). Apparently, for weak reflections, scanning of photon energy near the absorption edge can effectively suppress the scattering contributions from the iso-composition slabs (ICSS) of QDs with compositions close to that of shown matching points. The resonant x-ray diffraction method, due to the sensitivity to the density distribution of the resonant elements, thus, provides a high-resolution sectioning analysis for QDs structure.

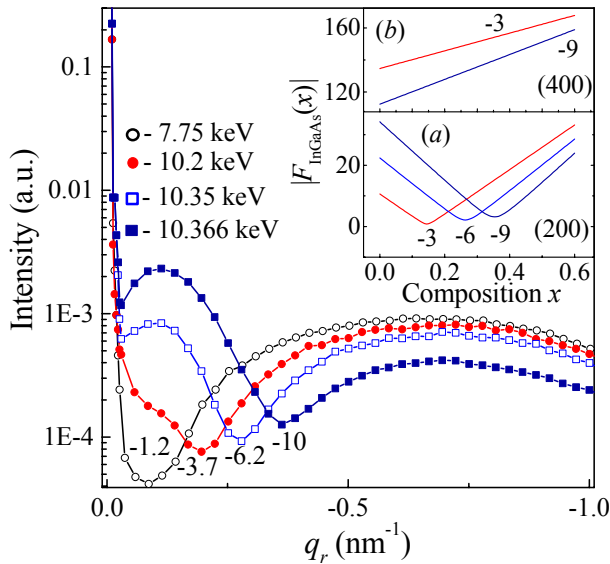


**Fig. 1:** Experimental radial intensity distributions  $I(q_r)$  measured for several energies of the incident radiation, with the corresponding  $f'$  values indicated near the curves. Insets: (a) The composition-dependent  $|F_{\text{InGaAs}}(x)|$  profiles calculated for the weak reflection (200) at three energies corresponding to  $f'$  values of -3, -6, and -9 near the Ga K-edge, respectively. (b) Similar calculations as that in (a) for the strong reflection (400).

The proposed approach was experimentally applied for self-assembled  $\text{In}_{0.5}\text{Ga}_{0.5}\text{As}$  QDs grown on GaAs(001) substrate by solid-source molecular-beam epitaxy. The scattering geometry with the crystallographic planes (200) normal to the surface (001) of substrate was set for an incident angle  $\alpha_i$  of  $0.19^\circ$ , which is less than the critical angle  $\alpha_c = 0.23^\circ$  of the total external reflection region for GaAs. The intensity distributions were measured along the radial  $q_r$  and angular  $q_a$  directions, and the exit angle  $\alpha_f$  using a linear detector. The  $q_r$  and  $q_a$  are the change of the momentum transfer with respect to the substrate reciprocal lattice vector  $\mathbf{Q}$  in the longitudinal and the transverse (in surface plane) directions. Fig. 1 shows the measured radial intensity distributions  $I(q_r)$  for several energies of the incident radiation in the vicinity of the Ga K-edge. These intensity distributions demonstrate the shifting of the intensity minimum due to the above-mentioned suppression of contributions from different ICSs of QDs [see the qualitative analogue with the shifting of the minimum for color curves in insert (a) of Fig. 1]. The presence of clearly discernable intensity minima for measured distributions shows a high structural perfection of investigated QDs. The radial position  $q_r$  of the intensity minimum obtained for the correspondent energy  $E$  gives a direct link between the lateral lattice parameter

$$a(q_r) = [a_{\text{GaAs}}^{-1} + q_r (2\pi\sqrt{h^2 + k^2 + l^2})^{-1}]^{-1} \quad (2)$$

of the iso-strain slab (ISS) and the averaged composition  $x(a)$  of this slab determined from the minimum of  $|F_{\text{InGaAs}}(x)|$  calculated for each energy.

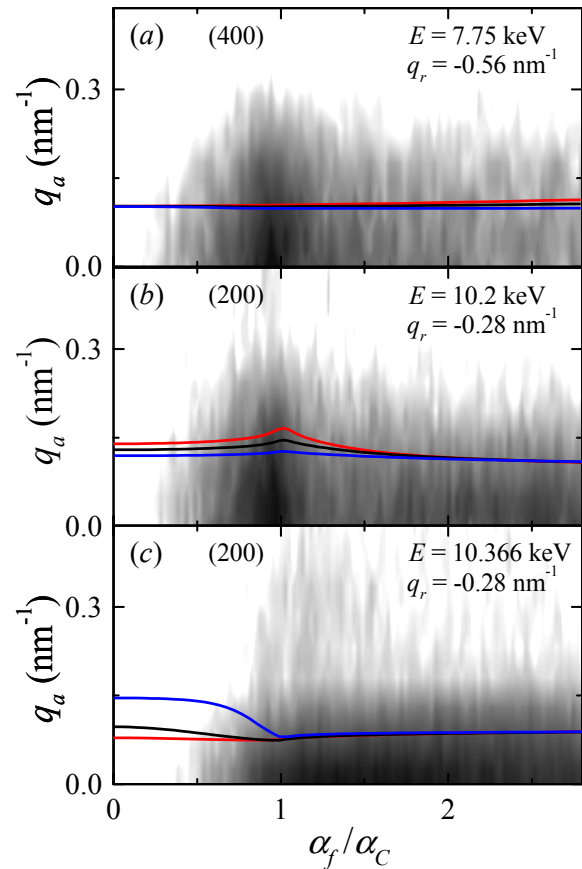


**Fig. 2:** Experimental  $I(q_a, \alpha_f)$  two-dimensional distributions measured for (a) the strong reflection (400) and (b) - (c) the weak reflection (200) at energies  $E$  and radial  $q_r$  positions indicated in figures. The color solid curves are the half-width  $W_a(\alpha_f)$  of the angular intensity distributions  $I(q_a)$  as functions of  $\alpha_f$ , simulated for several values of (a) the ISS curvature [red line -  $k_a(r) = 0 \text{ nm}^{-1}$ ; blue line -  $k_a(r) = 0.1 \text{ nm}^{-1}$ ] and (b) - (c) the ICS curvature [red line -  $k_x(r) = 0 \text{ nm}^{-1}$ ; blue line -  $k_x(r) = k_a(r)$ ]. The black solid curves are fitting results of the experimental  $W_a(\alpha_f)$  using DWBA simulations.

The proposed approach gives a highly sensitive correlation between the lateral lattice parameter  $a(q_r)$  and the averaged compositions of the ISSs. At the same time, the question of the composition variation within the ISS is of a great interest and importance. In the paper of Kegel *et al.*, [Phys. Rev. B **63**, 035318 (2001)] the spatial distribution of ISSs in QDs was obtained from the assumption that there is no lateral variation of composition in QDs. The proposed approach in our work is so sensitive to composition that it allows investigating the lateral distribution by the suppression of the diffraction contributions from regions of the ISS with different composition. On the other hand, the highly sensitive reflections complicate the understanding of the diffraction contributions from the curvatures of the ISSs and ICSs. For the separation of these contributions, the approach of employing strong reflections can be used. Due to their low sensitivity to composition [see insert (b) to Fig. 1], the lateral (and even the vertical) distribution of composition in QDs is not very important, and the information about the

curvature, size and height of ISSs slabs can be extracted. Fig. 2(a) shows the intensity distribution  $I(q_a, \alpha_f)$  experimentally measured for the strong reflection (400). The color lines, i.e., the half-width  $W_a$  of the angular  $q_a$  intensity distributions as functions of  $\alpha_f$ , simulated (within the framework of DWBA approximation) for several values of the ISS curvature and overlapped with the experimental data, show the general feature – the increase of the sensitivity of  $W_a(\alpha_f)$  to the ISS curvature with the increase of the exit angle  $\alpha_f$ . Fig. 3(b) displays the result of DWBA reconstruction of the spatial distribution of ISSs within QDs. This result was further used to extract information about spatial distribution of ICSs. Fig. 2(b) and (c) show the intensity distribution  $I(q_a, \alpha_f)$  measured for the weak reflection (200) using two energies close to the Ga  $K$ -edge. The simulations of the  $\alpha_f$  dependence of  $W_a$  [color lines in Fig. 2(b) and (c)] fulfilled for several values of the ICS curvature, indicate that in contrast to the above-mentioned feature, the total external reflection region,  $\alpha_f \leq \alpha_c$ , is now extremely sensitive to the value of ICS curvature. The dynamics of the  $W_a(\alpha_f)$  distribution change with the increase of the value of ICS curvature is following. In the first case, for the radial  $q_r$  ( $= -0.28 \text{ nm}^{-1}$ ) positions less than the radial position of the contrast-matching point ( $q_r = -0.2 \text{ nm}^{-1}$  for  $E = 10.2 \text{ keV}$ , see Fig. 1), the increase of the value of ICS curvature leads to the decrease of the width  $W_a(\alpha_f)$  [see Fig. 3(b)], while, in the second case, for  $q_r$  ( $= -0.28 \text{ nm}^{-1}$ ) positions more than the position of the contrast-matching point ( $q_r = -0.36 \text{ nm}^{-1}$  for  $E = 10.366 \text{ keV}$ , see Fig. 1), the same increase leads to the increase of  $W_a(\alpha_f)$  [see Fig. 2(c)]. This behaviour has a simple qualitative explanation. The speculative increase of the ICS curvature leads to quicker increase of composition  $x$  in rim regions of ISSs compare to their central (in the lateral direction) regions. In the first case, the narrowing of angular  $I(q_a)$  distributions is the result of the suppression of scattering contributions from central regions of ISSs with the lower composition  $x$ , while, in the second case, their broadening is the result of the

suppression of scattering contributions from rim regions with the higher composition. The result of DWBA reconstruction of the spatial distribution of ICSs within QDs is shown in Fig. 3(a). It was detected that the ICS curvature being nonzero is still smaller than that of the ISSs. In our representation the dimensionless  $\Delta a = (a - a_{\text{GaAs}}) / (a_{\text{InAs}} - a_{\text{GaAs}})$  is chosen deliberately in units equal under the Vegard's law to the composition  $x$  for an unstressed alloy. Fig. 3(a) and 3(b) show the dashed line where composition coincides with that of the unstressed alloy, that splits the dot into two regions, Region (I), dome-like area [ $0 < h < h_c$  in Fig. 3(c)] with the composition higher than that of the unstressed alloy (compressed material), which is covered by the layer, Region (II) [ $h > h_c$  in Fig. 3(c)] with a lower composition (tensile material). It is likely that the excess of InAs composition observed in Region (I), in comparison with the unstressed alloy, is imperative in overcoming the surface resistance of the GaAs substrate in the lateral direction. Whereas, the observed maximal composition  $x = 0.65$  at the top of QDs [Region (II)] is lower than that given by the Vegard's law. Nevertheless, it is still larger than the nominal growth value 0.5, manifesting an InAs-enrichment due to surface segregation.

In conclusion, we have shown that the use of weak reflections near the Ga  $K$ -absorption edge significantly enhances the accuracy of determination of the spatial distribution of composition within self-assembled InGaAs/GaAs QDs. By tuning the x-rays near the resonant energy, the proposed technique suppresses the diffraction contributions from neighbouring QD slabs of different compositions, thus, provides a way for high-resolution study of the QD structure. The structure reconstruction shows that the top layer of  $\text{In}_{0.5}\text{Ga}_{0.5}\text{As}/\text{GaAs}$  QDs of tensile material covers the intrinsic region of compressed material. The application of the proposed dispersive resonant x-ray diffraction technique can be extended for high-resolution studies of objects with a large gradient in composition, such as thin films and multilayers, for a wide class of systems.

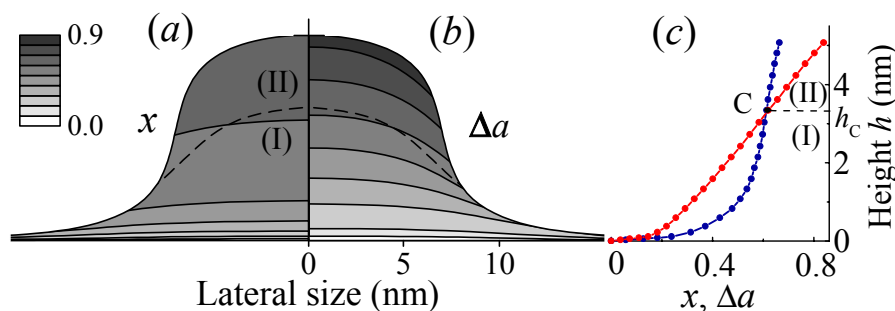


**Fig. 3:** Reconstructed spatial distributions of ICSs (a) and ISSs (b) within QDs. (c) The height-dependent distributions of the composition  $x$  (royal circles) and strain  $\Delta a$  (red circles) in the central region of QDs.

**BEAMLINE**

SP12B1 Materials X-ray Study beamline

17B1 W20 X-ray Scattering beamline

**EXPERIMENTAL STATION**

X-ray scattering end station

**AUTHORS**

Yu. P. Stetsko, C.-H. Hsu, M.-T. Tang and K. S. Liang

National Synchrotron Radiation Research Center,

Hsinchu, Taiwan

**PUBLICATIONS**

- C.-H. Hsu, H.-Y. Lee, Y.-W. Hsieh, Yu. P. Stetsko, M.-T. Tang, K.S. Liang, N. T. Yeh, J.-I. Chyi, and D. Y. Noh, *Physica B* **336**, 98 (2003).
- K. S. Liang, Yu. P. Stetsko, C.-H. Hsu, Y. Hwu, and D. Y. Noh, *Chinese Journal of Physics*, **43**, 219 (2005).
- Yu. P. Stetsko, C.-H. Hsu, M.-T. Tang, Y.-R. Lee, U. Jeng and K.S. Liang, *Phy. Rev. Lett.* (2005), submitted.

**CONTACT E-MAIL**

stetsko@nsrrc.org.tw